Sheffield Hallam University

A fast and parametric torque distribution strategy for four-wheel-drive energy-efficient electric vehicles

DIZQAH, Arash M, LENZO, Basilio <http://orcid.org/0000-0002-8520-7953>, SORNIOTTI, Aldo, GRUBER, Patrick, FALLAH, Saber and DE SMET, Jasper

Available from Sheffield Hallam University Research Archive (SHURA) at:

https://shura.shu.ac.uk/13970/

This document is the Accepted Version [AM]

Citation:

DIZQAH, Arash M, LENZO, Basilio, SORNIOTTI, Aldo, GRUBER, Patrick, FALLAH, Saber and DE SMET, Jasper (2016). A fast and parametric torque distribution strategy for four-wheel-drive energy-efficient electric vehicles. IEEE Transactions on Industrial Electronics, 63 (7), 4367-4376. [Article]

Copyright and re-use policy

See http://shura.shu.ac.uk/information.html

Sheffield Hallam University Research Archive
http://shura.shu.ac.uk

A Fast and Parametric Torque Distribution Strategy for Four-Wheel-Drive Energy Efficient Electric Vehicles

Arash M. Dizqah, *Member, IEEE*, Basilio Lenzo, *Member, IEEE*, Aldo Sorniotti, *Member, IEEE*, Patrick Gruber, Saber Fallah, Jasper De Smet

***Abstract*— Electric vehicles with four individually controlled drivetrains are over-actuated systems and therefore the total wheel torque and yaw moment demands can be realized through an infinite number of feasible wheel torque combinations. Hence, the energy-efficient torque distribution among the four drivetrains is crucial for reducing the drivetrain power losses and extending driving range. In this paper, the reference torque distribution is formulated as the solution of a parametric optimization problem, depending on vehicle speed. An analytical solution is provided for the case of equal drivetrains on the front and rear axles, under the experimentally confirmed hypothesis that the drivetrain power losses are monotonically increasing with the torque demand. The easily implementable and computationally fast wheel torque distribution algorithm is validated by simulations and experiments on an electric vehicle demonstrator, along driving cycles and cornering maneuvers. The results show considerable energy savings compared to alternative torque distribution strategies.**

***Index Terms*—Electric vehicle; torque distribution; control allocation; power loss; experiments.**

I. Introduction

One of the main obstacles to the success of electric vehicles (EVs) in the automotive market is their limited driving range. This issue is addressed by research in novel battery technologies to increase energy density and, hence, to provide viable/lightweight high-capacity energy storage systems. On the other hand, energy management systems are conceived to improve vehicle efficiency through advanced control of the drivetrains and ancillaries. In particular, EVs with multiple drivetrains allow the implementation of control functions, such as front-to-rear and left-to-right torque-vectoring, which improve active safety and drivability, and contribute to the attractiveness of EV technology [1-2]. Owing to the use of multiple motors an actuation redundancy is obtained – that is, the desired vehicle behavior corresponding to the driver's inputs at the accelerator/brake pedal and/or steering wheel can be realized through an infinite number of feasible wheel torque distributions. For the range of feasible torque distributions, this paper presents a novel solution to determine the combinations providing maximum energy efficiency.

The two major sources of power loss in EVs are the drivetrains and the tires. The drivetrain power losses include the contributions of the drives, electric motors and transmissions (where present). Tire contributions relate to rolling resistance, longitudinal slip and lateral slip, with the latter two being relevant only at significant acceleration levels.

Prior research (e.g., [3-7]) indicates that the power losses can be reduced by specific torque distribution algorithms, also called control allocation (CA) strategies. For instance, [3,8] present CA strategies minimizing energy dissipation due to tire slip. Although effective, the practical implementation of these strategies requires some form of continuous estimation of the longitudinal and lateral slip velocities of each tire, which is beyond the capability of existing state estimators in normal driving conditions. In [4-6] and [9-11] the reduction of energy dissipations within the electric motor drives is examined. The presented strategies are mainly based on experimentally measured efficiency maps of electric motors. In particular, [4] carries out an off-line calculation of the optimal wheel torques, but without analyzing the resulting wheel torque distribution as a function of the input parameters, i.e., wheel torque demand and vehicle speed. The results in [4] imply that the optimal solution is either to only use a single axle or to evenly distribute the torque among the four drives of the EV. Moreover, the CA strategies in [5,11-12] are shown to be more efficient than simple even torque distribution among the front and rear axles. However, the influence of vehicle speed (V) on the optimal solution is not directly taken into account. The effect of speed variation is investigated in [6] but it is not formulated. [9] discusses the change of the optimal distribution ratio as a function of longitudinal acceleration. The problem formulation is novel with results indicating small variations of the optimal distribution ratio over the achievable acceleration range. According to the results in [9], the vehicle never operates in the 'single-axle' mode, which is shown in [4,7] to be the optimal solution for small torque demands. Also, [9] only considers straight line driving. [10] presents a CA strategy that is based on a simplified piecewise-linear efficiency map of the brushless DC motors. An algorithm, based on Karush-Kuhn-Tucker (KKT) conditions of optimality, finds global solutions of the CA problem for non-monotonically increasing drivetrain power loss curves. The corresponding non-convex optimization problem is translated into a number of equivalent eigenvalue problems. [13-14] propose high-level controllers aimed at achieving the reference cornering response, coupled with CA algorithms to improve vehicle stability. However, [3] shows that such

strategies can be far from optimal in terms of energy efficiency.

In summary, an extensive literature deals with the subject of CA strategies for four-wheel-drive EVs. Many of the proposed algorithms are designed for reduced tire slip variance among the wheels. The papers dealing with drivetrain energy efficiency either do not discuss the resultant wheel torque distribution maps, or they present very complicated algorithms (such as multi-parametric non-convex optimization, [15-16]), which are unlikely to be directly implemented on production vehicles. As a consequence, there is a clear need for simple, computationally efficient, easily-tunable and effective solutions of the CA problem aimed at energy efficiency. The gap is addressed by this paper, including the following novel contributions:

i) The analytical solution of the CA problem maximizing energy efficiency, under the hypothesis of monotonically increasing drivetrain power losses with torque demand. The optimal solution, obtained for the case of equal drivetrains on the front and rear axles, is parameterized as a function of V;
ii) A fast and easily implementable torque distribution strategy maximizing energy efficiency, based on the proposed analytical solution in i);
iii) The simulation-based and experimental validation of the energy benefits of the CA algorithm in cornering conditions and along driving cycles.

The remainder of the paper is organized in four sections (II to V). Section II formulates the energy-efficient CA problem as a multi-parametric non-convex optimization. Section III provides the theoretical background required to design the proposed fast CA for EVs. The performance of the CA strategy is verified in Section IV through computer simulations with a vehicle dynamics model and experiments on an electric Range Rover Evoque demonstrator vehicle. Finally, the conclusions are provided in Section V.

II. Problem Statement and Formulation

A. Problem statement

Fig. 1 shows the simplified vehicle control structure. The reference generator outputs the reference yaw rate, r_{ref}, and traction/braking force, F_{ref}, starting from the steering wheel angle (δ), accelerator and brake pedal positions (respectively APP and BPP), and longitudinal vehicle speed and acceleration (respectively V and a_x). The high-level controller calculates the corrected longitudinal force reference, $\tilde{F}_{ref}$ (i.e., F_{ref} from the reference generator is reduced in extreme cornering conditions), and the yaw moment reference, ΔM_{ref}, e.g., based on the combination of feedforward and feedback control of vehicle yaw rate, r.

The proposed CA strategy must minimize the drivetrain energy consumption while maintaining $\tilde{F}_{ref}$ (each drivetrain can operate in either traction or regeneration) and ΔM_{ref}. As the drivetrain power losses are functions of V, the CA strategy includes V as a parameter.

The CA problem is formulated as a static optimization or quasi-dynamic optimization [17-19] to be solved at each time step for the values of $\tilde{F}_{ref}$ and ΔM_{ref} calculated by the high-level controller, and the estimated V (Fig. 1). The CA strategy could be integrated into the high-level controller, thus giving origin to a single multiple-output controller. On the other hand, the separation among the high-level controller and the CA strategy (Fig. 1) has advantages, such as ease of considering actuator limitations [20] and flexibility with respect to the drivetrain configuration. The following subsection will formulate the CA problem mathematically, under Assumptions 1 and 2.

Assumption 1: The case study EV includes four identical electric drivetrains with equal power loss characteristics – i.e., the electric machines and their power electronics, single-speed gearboxes, constant-velocity joints and wheels are the same on each vehicle corner.

Assumption 2: The drivetrain power loss characteristic on each vehicle corner, $P_{loss}(\tau_w, V)$, is positive and monotonically increasing as a function of torque demand, τ_w. This means that $P_{loss}(\tau_w, V) > 0$ and $\partial P_{loss}(\tau_w, V)/\partial \tau_w \geq 0$.

The results presented in the next paragraphs can also be applied (with specific re-arrangements) to the simplified case of a four-wheel-drive EV with a single drivetrain per axle.

B. Mathematical formulation

The proposed optimal CA problem for small steering angles is formulated as follows:

$$
\begin{aligned}
\{\tau_w\}^*(\tilde{F}_{ref}, \Delta M_{ref}, V) &= \arg \min_{\tau_{w_{i,t}}, \tau_{w_{i,g}}} J\left(\tau_{w_{i,t}}, \tau_{w_{i,g}}, V\right) \\
&:= \sum_{i=1}^{4} \left[P_{i,t}\left(\tau_{w_{i,t}}, V\right) - P_{i,g}\left(\tau_{w_{i,g}}, V\right)\right] \\
s.t. \quad & \textstyle\sum_{i=1}^{4}\left(\tau_{w_{i,t}} - \tau_{w_{i,g}}\right) = \tilde{F}_{ref} R \\
& d_f\left(\tau_{w_{2,t}} + \tau_{w_{1,g}} - \tau_{w_{1,t}} - \tau_{w_{2,g}}\right) + \\
& d_r\left(\tau_{w_{4,t}} + \tau_{w_{3,g}} - \tau_{w_{3,t}} - \tau_{w_{4,g}}\right) = \Delta M_{ref} R \\
& 0 \leq V \leq V_{max} \\
& 0 \leq \tau_{w_{i,t}} \leq \tau_{w,max,i,t} \\
& 0 \leq \tau_{w_{i,g}} \leq \tau_{w,max,i,g} \\
& \tau_{w_{i,t}} \tau_{w_{i,g}} = 0; \; i = 1,2,3,4
\end{aligned}
\tag{1}
$$

$\tau_{w_{i,t}}$ and $\tau_{w_{i,g}}$ are the traction and regeneration torques at

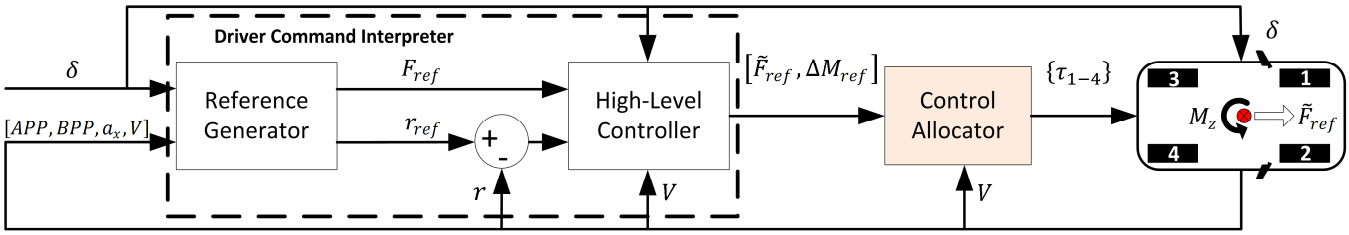

Fig. 1. The vehicle dynamics control structure

the different wheels (numbered as in Fig. 1). R is the tire radius. d_f and d_r are the front and rear half-tracks. $\tau_{w,max,i,t}$ and $\tau_{w,max,i,g}$ are the minimum between the torque available at the drivetrain in traction, $\tau_{w,max,t}(V)$, or regeneration, $\tau_{w,max,g}(V)$, and the transmissible torque at the tire-road contact, $\mu F_{z,i} R$, being μ the estimated tire-road friction coefficient and $F_{z,i}$ the estimated vertical load at the wheel i. The first and second constraint in (1) have a clear physical meaning in vehicle dynamics: they require that the torques applied at the wheels generate, respectively, the reference longitudinal force of the vehicle $\tilde{F}_{ref}$, and the reference yaw moment of the vehicle ΔM_{ref}.

In the hypothesis of low load transfers, Problem (1) has three parameters: i) $\tilde{F}_{ref}$; ii) ΔM_{ref} and iii) vehicle speed. The problem is non-convex due to the complementarity constraints and non-convexities in the power loss characteristics of the electric machines and mechanical transmission systems. The complementarity constraints $\tau_{w_{i,t}} \tau_{w_{i,g}} = 0$ specify that at each instant each wheel can only operate in traction or regeneration. $P_{i,t}$ and $P_{i,g}$ are, respectively, the drawn and regenerated electrical powers at the wheel i, given by:

$$\begin{aligned} P_{i,t} &= \tau_{w_{i,t}} \frac{V}{R} + P_{loss,t}\left(\tau_{w_{i,t}}, V\right);\ i = 1,2,3,4 \\ P_{i,g} &= \tau_{w_{i,g}} \frac{V}{R} - P_{loss,g}\left(\tau_{w_{i,g}}, V\right);\ i = 1,2,3,4 \end{aligned} \tag{2}$$

where the first term on the right-hand side is the mechanical power and the second term is the power loss. The power losses of all vehicle corners are modeled with the same functions, $P_{loss,t/g}$ (the subscripts indicate traction and regeneration, respectively), obtained by fitting the experimental measurements on the drivetrains to a mathematical expression (Assumption 1).

By replacing (2) into the cost function $J\left(\tau_{w_{i,t}}, \tau_{w_{i,g}}, V\right)$ of (1), J is reformulated as:

$$J\left(\tau_{w_{i,t}}, \tau_{w_{i,g}}, V\right) = \frac{V}{R}\left(\frac{\tilde{F}_{ref} R}{\sum_{i=1}^{4}\left(\tau_{w_{i,t}} - \tau_{w_{i,g}}\right)}\right) + \sum_{i=1}^{4}\left[P_{loss,t}\left(\tau_{w_{i,t}}, V\right) + P_{loss,g}\left(\tau_{w_{i,g}}, V\right)\right] \tag{3}$$

where the first term on the right-hand side is the overall mechanical power and the second term is the overall power loss.

The term $(V/R)\tilde{F}_{ref} R$ can be assumed constant for any value of the parameters. Hence, the cost function can be reduced to:

$$J\left(\tau_{w_{i,t}}, \tau_{w_{i,g}}, V\right) = \sum_{i=1}^{4}\left[P_{loss,t}\left(\tau_{w_{i,t}}, V\right) + Ploss,g\tau wi,g,V\right. \tag{4}$$

(4) assumes that the vehicle operates with limited yaw rate and limited relative slip among the wheels, which means that V can be used as the speed of each vehicle corner.

In summary, (1) is a multi-parametric Non-Linear Programming (mp-NLP) problem [21-22], with the following general formulation:

$$\begin{aligned} z(\theta) &= \min_{x \in X} J(x, \theta) \\ s.t.\ & G(x, \theta) \le 0; H(x, \theta) = 0;\ \theta \in \Theta \end{aligned} \tag{5}$$

where $\theta = \left[\tilde{F}_{ref}, \Delta M_{ref}, V\right]^T$ is the parameter vector, and G and H represent the inequality and equality constraints.

III. Controller design

Lemma 1: Problem (1) has only one solution for each side of the vehicle, assuming $d = d_f = d_r$:

$$\begin{aligned} \tau_{w,l}^* &= 0.5\left(\tilde{F}_{ref} - \frac{\Delta M_{ref}}{d}\right) R; \\ \tau_{w,r}^* &= 0.5\left(\tilde{F}_{ref} + \frac{\Delta M_{ref}}{d}\right) R; \\ -\tau_{w,max,l,g} &\le \tau_{w,l}^* \le \tau_{w,max,l,t}; \\ -\tau_{w,max,r,g} &\le \tau_{w,r}^* \le \tau_{w,max,r,t} \end{aligned} \tag{6}$$

where $\tau_{w,l}^*$ and $\tau_{w,r}^*$ are, respectively, the reference wheel torques of the left- and right-hand sides of the vehicle, with $\tau_{w,max,l,t/g} = \tau_{w,max,1,t/g} + \tau_{w,max,3,t/g}$ and $\tau_{w,max,r,t/g} = \tau_{w,max,2,t/g} + \tau_{w,max,4,t/g}$ (the subscripts 't' and 'g' indicate traction and regeneration, respectively).

Proof: From the vehicle schematic in Fig. 1:

$$\begin{aligned} \tau_{w,l} &= \tau_{w_{1,t}} + \tau_{w_{3,t}} - \tau_{w_{1,g}} - \tau_{w_{3,g}} \\ \tau_{w,r} &= \tau_{w_{2,t}} + \tau_{w_{4,t}} - \tau_{w_{2,g}} - \tau_{w_{4,g}} \end{aligned} \tag{7}$$

By replacing (4) and (7) into (1), Problem (1) becomes:

$$\begin{aligned} \{\tau_w\}^*\left(\tau_{ref}, \Delta M_{ref}, V\right) &= \arg\min_{\tau_{w,l}, \tau_{w,r}} J\left(\tau_{w,l}, \tau_{w,r}, V\right) \\ &:= P_{loss_l}\left(\tau_{w,l}, V\right) + P_{loss_r}\left(\tau_{w,r}, V\right) \\ s.t.\quad \tau_{w,l} + \tau_{w,r} &= \tilde{F}_{ref} R; \\ \tau_{w,r} - \tau_{w,l} &= \frac{\Delta M_{ref} R}{2d}; \end{aligned} \tag{8}$$

$$0 \le V \le V_{max};$$
$$-\tau_{w,max,l,g} \le \tau_{w,l} \le \tau_{w,max,l,t};$$
$$-\tau_{w,max,r,g} \le \tau_{w,r} \le \tau_{w,max,r,t}$$

The complementarity conditions $\tau_{w_{i,t}}\tau_{w_{i,g}} = 0$ are no longer present in (8) as they are internal conditions for the left- and right-hand sides; this implies that $\tau_{w,l}$ and $\tau_{w,r}$ can only vary between $-\tau_{w,max,l/r,g}$ and $\tau_{w,max,l/r,t}$ (the subscripts 'l' and 'r' indicate left and right, respectively). Problem (8) has a unique solution, as in (6), due to the two equality constraints for the decision variables $\tau_{w,l}$ and $\tau_{w,r}$. The solution is fixed and independent of the cost function. □

Remark 1: The solutions for the left- and right-hand sides of the vehicle are independent of V and only depend on $\tilde{F}_{ref}$ and ΔM_{ref}.

Remark 2: The reference values of the total longitudinal force and yaw moment are restricted by the maximum and minimum torques of the electric motors, which depend on V, and (in second approximation) the estimated tire-road friction coefficient.

Remark 3: As mentioned before, because of the two equality constraints with two decision variables in the main problem, a unique analytical feasible solution exists. To consider torque rate constraints, these two equality constraints need to be relaxed or transferred to the cost function to make the problem feasible.

Lemma 2: If Assumptions 1 and 2 hold, the optimal torque distributions for the left- or right-hand sides of the vehicle make both front and rear motors work in either traction or regeneration (including the case that one motor is switched off and only one motor is producing torque).

Proof: Lemma 1 proves that Problem (1) can be simplified to an optimal torque distribution problem for each side of the vehicle. The optimal torque distribution of the left-hand side of the vehicle for the case of traction, i.e., $\tau^*_{w,l} \ge 0$, is the solution of the following problem:

$$\begin{aligned}\{\tau_w\}^*(\tau_{w,l},V) = \arg \min_{\tau_{w_{1,t}},\tau_{w_{3,t}},\tau_{w_{1,g}},\tau_{w_{3,g}}} & P_{loss,t}(\tau_{w_{1,t}},V) \\ & + P_{loss,t}(\tau_{w_{3,t}},V) + P_{loss,g}(\tau_{w_{1,g}},V) \\ & + P_{loss,g}(\tau_{w_{3,g}},V)\end{aligned} \tag{9}$$

$$\begin{aligned} s.t.\quad & \tau_{w_{1,t}} + \tau_{w_{3,t}} - \tau_{w_{1,g}} - \tau_{w_{3,g}} = \tau^*_{w,l}; \\ & \tau_{w_{i,t}}\tau_{w_{i,g}} = 0;\ i \in \{1,3\}; \\ & 0 \le \tau_{w_{i,g}} \le \tau_{w,max,i,g}; \\ & 0 \le \tau_{w_{i,t}} \le \tau_{w,max,i,t}\end{aligned}$$

The same problem is defined for the right-hand side of the vehicle or for the regeneration case, i.e., $\tau^*_{w,l} < 0$. Expanding the complementarity constraint of Problem (9), the optimal solution of (9) is the best solution among the following four problems:

$$\begin{aligned}&\{\tau_w\}^*(\tau_{w,l},V) \\ &= \arg \min_{\tau_{w_1},\tau_{w_3}} P_{loss,t/g}(\tau_{w_1},V) + P_{loss,t/g}(\tau_{w_3},V) \\ &\quad s.t.\ \begin{cases} \tau_{w_1} + \tau_{w_3} = \tau^*_{w,l}; OR \\ -\tau_{w_1} - \tau_{w_3} = \tau^*_{w,l}; OR \\ \tau_{w_1} - \tau_{w_3} = \tau^*_{w,l}; OR \\ -\tau_{w_1} + \tau_{w_3} = \tau^*_{w,l}. \end{cases} \\ &\qquad 0 \le \tau_{w_i} \le \tau_{w,max,i,t}\ OR \\ &\qquad 0 \le \tau_{w_i} \le \tau_{w,max,i,g};\ i \in \{1,3\}\end{aligned} \tag{10}$$

where τ_{w_1} and τ_{w_3} are the torques at the left front and left rear wheels. $\tau_{w_1} + \tau_{w_3} = \tau^*_{w,l}$ and $-\tau_{w_1} - \tau_{w_3} = \tau^*_{w,l}$ represent the pure traction and regeneration cases, while $\tau_{w_1} - \tau_{w_3} = \tau^*_{w,l}$ and $-\tau_{w_1} + \tau_{w_3} = \tau^*_{w,l}$ are the cases in which one of the wheels is in traction and the other one in regeneration.

The resulting value of the cost function in (10) is smaller without regeneration as P_{loss} is positive and monotonically increasing, i.e., $P_{loss} \ge 0$ and $\partial P_{loss}/\partial \tau_w \ge 0$ (Assumption 2). Any regeneration increases the absolute value of the traction torque and therefore, according to (2), increases the total power loss. As a result, the conditions $\tau_{w_1} - \tau_{w_3} = \tau^*_{w,l}$ and $-\tau_{w_1} + \tau_{w_3} = \tau^*_{w,l}$ are not optimal cases and, depending on the sign of $\tau^*_{w,l}$, both wheels on the same side must work in either traction or regeneration.

□

Theorem 1: Suppose that Assumptions 1 and 2 hold, $P_{loss}(\tau_w)$ has the shape indicated in Fig. 2 (with a non-convex region followed by a convex region, i.e., with a single saddle point) and there are no torque rate constraints; then for each side of the vehicle:

a) Single-axle is the optimal solution for small values of the reference torque demand;
b) Even distribution among the wheels is the optimal solution for large values of the reference torque demand;
c) The optimal switching point between strategies a) and b) at vehicle speed V can be calculated as the solution of:

$$\begin{aligned}&P_{loss,t/g}(\tau_{sw},V) + P_{loss,t/g}(0,V) = \\ &\quad 2P_{loss,t/g}(0.5\tau_{sw},V)\end{aligned} \tag{11}$$

where τ_{sw} is the switching torque.

Proof: Lemma 2 proves that the optimal torque distribution of the left-hand side of the vehicle with $\tau^*_{w,l} \ge 0$ is the solution of the following problem:

$$\begin{aligned}\{\tau_w\}^*(\tau_{w,l},V) = \arg \min_{\tau_{w_1},\tau_{w_3}} & J(\tau_{w_1},\tau_{w_3},V) \\ := & P_{loss,t}(\tau_{w_1},V) + P_{loss,t}(\tau_{w_3},V)\end{aligned} \tag{12}$$

$$\begin{aligned} s.t.\quad & \tau_{w_1} + \tau_{w_3} = \tau^*_{w,l}; \\ & 0 \le \tau_{w_i} \le \tau_{w,max,i,t};\ i \in \{1,3\}.\end{aligned}$$

By approximating the cost function of (12) around $\tau_{w,0} = \tau^*_{w,l}/2$, which is the solution of the even distribution strategy, the Taylor series is:

$$\begin{aligned}&J(\tau_{w_1},\tau_{w_3},V) \cong \\ &P_{loss,t}(\tau_{w,0},V) + \nabla_{\tau_w} P_{loss,t}(\tau_{w,0},V)(\tau_{w_1} - \tau_{w,0}) +\end{aligned} \tag{13}$$

$$\frac{1}{2}\nabla^2_{\tau_w\tau_w}P_{loss,t}(\tau_{w,0},V)(\tau_{w_1}-\tau_{w,0})^2 + P_{loss,t}(\tau_{w,0},V) + \nabla_{\tau_w}P_{loss,t}(\tau_{w,0},V)(\tau_{w_3}-\tau_{w,0}) + \frac{1}{2}\nabla^2_{\tau_w\tau_w}P_{loss,t}(\tau_{w,0},V)(\tau_{w_3}-\tau_{w,0})^2$$

Since $\tau_{w_1}+\tau_{w_3}=\tau^*_{w,l}$ is a constant value, if τ_{w_1} (or τ_{w_3}) deviates from $\tau_{w,0}$ by the amount ε, then τ_{w_3} (or τ_{w_1}) must deviate from $\tau_{w,0}$ by the same amount but in opposite direction:

$$\tau_{w_1}=\tau_{w,0}+\varepsilon;\ \tau_{w_3}=\tau_{w,0}-\varepsilon \tag{14}$$

By substituting (14) into (13), the Taylor series approximation in (13) is reformulated as:

$$J(\varepsilon,V)\cong 2P_{loss,t}(\tau_{w,0},V)+\nabla^2_{\tau_w\tau_w}P_{loss,t}(\tau_{w,0},V)\varepsilon^2 \quad s.t.\quad -\tau_{w,0}\le\varepsilon\le\tau_{w,0} \tag{15}$$

$2P_{loss}(\tau_{w,0},V)$ is the power loss of the even distribution case. Therefore, for $P_{loss}\ge 0$:

- If the Hessian of P_{loss} is negative, i.e., P_{loss} is non-convex at $\tau_{w,0}$, then $J(\varepsilon,V)<2P_{loss}(\tau_{w,0},V)$ and, therefore, the even distribution is the worst strategy. In this case the minimum value of the cost function is achieved with the biggest offset from $\tau_{w,0}$. From Lemma 2 (see also Fig. 2), the biggest offset is for the case $|\varepsilon|=\tau_{w,0}$, and therefore τ_{w_1} or τ_{w_3} must be zero, which is equivalent to the single-axle strategy a);
- If the Hessian of P_{loss} is positive or zero at $\tau_{w,0}$, i.e., P_{loss} is convex at $\tau_{w,0}$, then $J(\varepsilon,V)\ge 2P_{loss}(\tau_{w,0},V)$, which means that the even distribution ($\varepsilon=0$) is the optimal solution. Fig. 2 shows that P_{loss} is typically convex for large torque demands and therefore b) is proven.

If both $\tau_{w,0}$ and $\tau_{w,0}+min\{\varepsilon\}$ are in the convex region of Fig. 2, the even distribution becomes the optimal strategy. On the other hand, if both $\tau_{w,0}$ and $\tau_{w,0}+max\{\varepsilon\}$ fall in the non-convex area, the single-axle is the optimal strategy. As a result, an optimal switching torque τ_{sw} between these two strategies can be found – that is, a torque value exists at which the power loss of the even distribution strategy, $2P_{loss}(0.5\tau_{sw},V)$, is equal to the one of the single-axle strategy, $P_{loss}(\tau_{sw},V)+P_{loss}(0,V)$.

□

Fig. 2 represents a geometrical interpretation of the optimal switching torque, τ_{sw}. It shows that the single-axle strategy is the optimal one up to the point at which $P_{loss}(2\tau_w,V)-P_{loss}(\tau_w,V)\le P_{loss}(\tau_w,V)-P_{loss}(0,V)$. The right- and left-hand sides of the inequality are, respectively, the amount of power loss which is reduced, compared to the even distribution, by switching off one of the drivetrains, and the amount of power loss increase by the other drivetrain, again compared to the even distribution. Suppose Assumption 2 holds, these two terms become equal at the switching torque τ_{sw}.

Remark 4: Based on Theorem 1, the optimal distribution strategy is as follows:

$$\tau^*_{w,1}(\tau^*_{w,l},V)=\begin{cases}\tau^*_{w,l} & \tau^*_{w,l}\le\tau_{sw}(V)\\ 0.5\tau^*_{w,l} & \tau^*_{w,l}>\tau_{sw}(V)\end{cases}$$
$$\tau^*_{w,3}(\tau^*_{w,l},V)=\begin{cases}0 & \tau^*_{w,l}\le\tau_{sw}(V)\\ 0.5\tau^*_{w,l} & \tau^*_{w,l}>\tau_{sw}(V)\end{cases} \tag{16}$$

where $\tau^*_{w,1}$ and $\tau^*_{w,3}$ are, respectively, the optimal torque demands of the front and rear wheels of the left-hand side of the vehicle. In the single-axle strategy the front motors are selected (instead of the rear motors) for safety reasons; in fact, in limit conditions it is preferable to have understeer rather than oversteer.

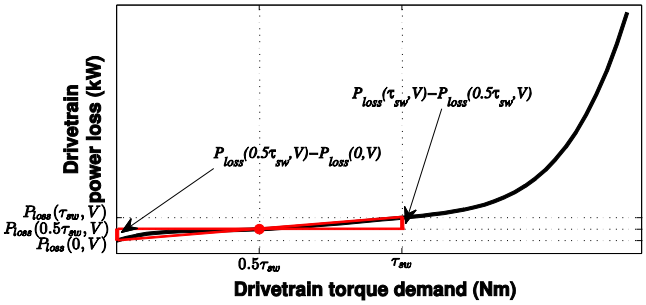

Fig. 2. Geometrical interpretation of Theorem 1, indicating the optimal switching point on the drivetrain power loss characteristic

The equivalent right-hand side torques are calculated with the same approach. In the practical implementation of the controller, a sigmoid function is used to approximate the discontinuity of (16), in order to prevent drivability issues deriving from the fast variation of the torque demands.

Remark 5: τ_{sw} depends on the value of V. Since the problem is parametric, the solution is parametric as well. In practice, V can be estimated with a suitable Kalman filter using the four wheel speed signals and the longitudinal acceleration of the vehicle [23-24].

Remark 6: If $P_{loss}(\tau_w)$ is convex (i.e., without the saddle point in Fig. 2), then the even distribution is the optimal solution for any torque demand.

Remark 7: If (13) is not a good approximation of $J(\tau_{w_1},\tau_{w_3},V)$, the even order derivatives of $P_{loss,t}(\tau_w,V)$ with respect to τ_w must either be zero or have the same sign for the same values of τ_w. For example, this is the case if $P_{loss,t}(\tau_w,V)$ is a cubic polynomial. The experimental power loss characteristics reported in Section IV are very well interpolated by a cubic polynomial.

Remark 8: Theorem 1 can be extended to the case of a $P_{loss}(\tau_w)$ characteristic with multiple saddle points (i.e., with a sequence of several non-convex and convex parts), maintaining the assumption that P_{loss} is monotonically increasing.

Remark 9: The developed control allocation strategy is overruled in two cases:

- In the case of wheel torque saturation (see Section II.B), the torque demand beyond the limit is transferred to the

other wheel on the same side until saturation is reached as well;

- For significant braking, an Electronic Braking Distribution (EBD) strategy intervenes to maintain the correct relative slip ratio among the tires of the front and rear axles.

IV. Results

A. Experiments

Experimental system setup

Fig. 3 shows the experimental set-up for the validation of the developed torque distribution strategy. The vehicle demonstrator is an electric Range Rover Evoque with four identical on-board switched reluctance motors, connected to the wheels through single-speed transmissions, constant-velocity joints and half-shafts. Table 1 reports the main vehicle parameters.

A dSPACE AutoBox system is used for running all controllers (Fig. 1), including the reference generator, the high-level controller (as in [23]) and the CA algorithm. The electrical power is provided by an external supply (visible in the background of Fig. 3), which is connected in parallel with the battery pack. Therefore, the high-voltage dc bus level is maintained steady around 600 V.

The tests are conducted using a MAHA rolling road facility (located at Flanders MAKE, Belgium) allowing speed and torque control modes of the rollers. In the speed control mode, the roller speeds are constantly kept at the specified set value irrespective of variations in the actual wheel torques. The torque demand at each wheel is assigned manually through the dSPACE interface, and therefore the vehicle can be tested for any assigned achievable torque demand and speed. The rig includes the measurement of the longitudinal force and speed of the rollers, and thus allows the evaluation of the overall drivetrain efficiency, i.e., from the electrical power at the inverters to the mechanical power at the rollers during traction (opposite flow in the case of regeneration). In the torque control mode, the roller bench applies a torque to the rollers, which emulates tire rolling resistance, aerodynamic drag and vehicle inertia. Therefore, the torque control mode is used for driving cycle testing. The vehicle follows the reference velocity profile of the specific driving schedule through a velocity trajectory tracker (i.e., a model of the human driver) implemented on the dSPACE system as the combination of a feedforward and feedback controller, providing a wheel torque demand output.

Drivetrain power loss measurement

The experimental drivetrain power loss characteristics of the case study EV are reported in Fig. 4 for a number of vehicle speeds. The power loss curves are plotted in terms of the actual wheel torque. The first point of each curve corresponds to the case of zero torque demand, resulting in non-zero power loss due to tire rolling resistance; conversely, the actual wheel torque is zero when the torque supplied by drivetrain compensates rolling resistance.

Fig. 4 shows that the drivetrain power loss characteristics are positive and monotonically increasing functions of wheel torque, hence, confirming Assumption 2. The curves are non-convex for low wheel torques and become convex for large torque values. Therefore, Theorem 1 is applicable to the design of an energy-efficient CA algorithm for the electric Range Rover Evoque demonstrator. Fig. 5 reports the measured efficiencies of each side of the EV demonstrator in terms of the front-to-total torque ratio, for different values of V and side torque demands. The relative slip among the wheels did not change significantly for different combinations of speeds, torque demands and front-to-total torque ratios. Due to the non-convexity of the power loss at low torque demands, the efficiency is higher for torque ratios of 0 or 1, i.e., for the single-axle strategy. In contrast, an even distribution (corresponding to the torque ratio of 0.5) is the optimal solution for high torque demands. As a result, the optimal torque distribution on each side of the vehicle is achieved by switching between the single-axle and even torque distributions depending on torque demand and vehicle speed.

TABLE 1
Main vehicle parameters

Symbol	Name and dimension	Value
ℓ	Wheelbase (m)	2.665
τ_{gb}	Gearbox ratio (-)	10.56
R	Wheel radius (m)	0.364
d	Half-track (m)	0.808
–	No. of motors per axle (-)	2
V_{dc}	High-voltage dc bus level (V)	600
T_n	Motor nominal torque (Nm)	80
P_n	Motor nominal power (kW)	35
P_p	Motor peak power (kW)	75

Fig. 3. The Range Rover Evoque set-up on the rolling road facility at Flanders MAKE (Belgium)

Switching torque calculation

Based on the measured power loss curves in Fig. 4, the switching torque, τ_{sw}, is calculated using Theorem 1 and (11). The power loss curve at each vehicle speed is piecewise linearly interpolated to construct $P_{loss}(\tau_w, V)$, as in (4). The method assumes that the tire rolling resistance power losses are equal at each vehicle corner, which is a reasonable approximation in normal driving conditions with low values of the load transfers (which directly affect tire power losses). The longitudinal slip power losses are included in the rolling road measurement. The method assumes that the slip ratios are similar to those measured on the rolling road, which is also a

reasonable approximation in normal driving conditions. Knowing $P_{loss}(\tau_w, V)$, (11) is solved offline with an exhaustive search method to calculate τ_{sw}. Fig. 6 shows the calculated τ_{sw} on each side of the vehicle for different V. The values are stored as a look-up table in the controller implemented on the dSPACE system. In terms of implementation on the vehicle, the developed procedure was demonstrated to be fast, i.e. it can easily be run in real-time on hardware with low computational processing power.

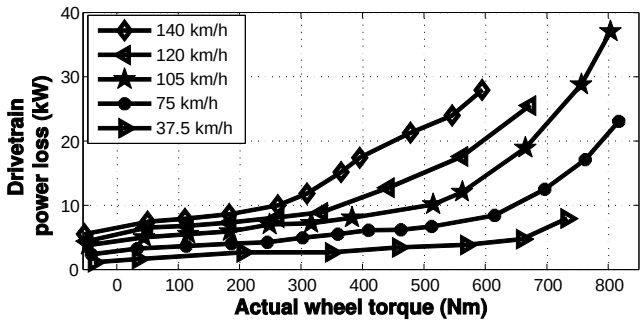

Fig. 4. The power losses of a single drivetrain, measured on the rolling bench facility

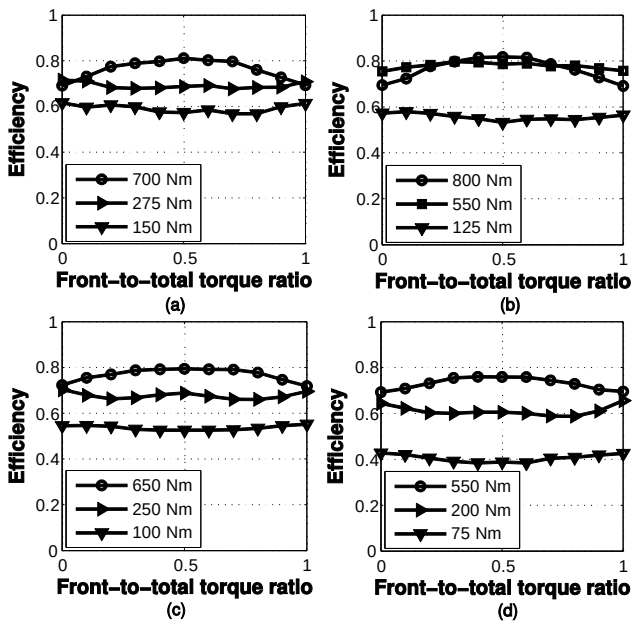

Fig. 5. Measured drivetrain efficiencies as a function of the front-to-total torque ratio, for different side torques at vehicle speeds of: (a) 40 km/h; (b) 65 km/h; (c) 90 km/h; and (d) 115 km/h

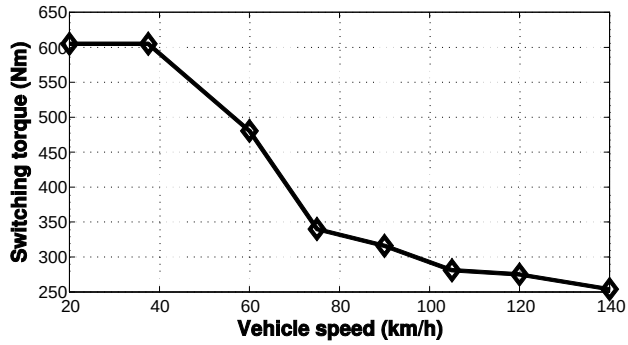

Fig. 6. Switching torque (τ_{sw}) for each side of the vehicle as a function of V

Driving cycle tests

To assess the energy-efficiency benefits of the developed CA strategy in straight line conditions, three different driving cycles were performed with the vehicle demonstrator on the rolling road. The driving cycles are the New European Driving Cycle (NEDC), the Artemis Road driving cycle, and the Extra Urban Driving Cycle (EUDC) with the hypothesis of a constant 8% (uphill) slope of the road.

TABLE 2
ENERGY CONSUMPTION OF THE DEVELOPED CONTROL ALLOCATION STRATEGY OVER DIFFERENT DRIVING CYCLES

Driving Cycle	Energy consumptions (kWh)			Improvements (%) by CA with respect to	
	Single-axle only	Even distribution	With CA	Single-axle only	Even distribution
NEDC	2.921	3.059	2.918	0.1%	4.6%
Artemis-Road	4.487	4.634	4.442	1.0%	4.1%
EUDC 8% slope	5.793	5.740	5.709	1.5%	0.5%

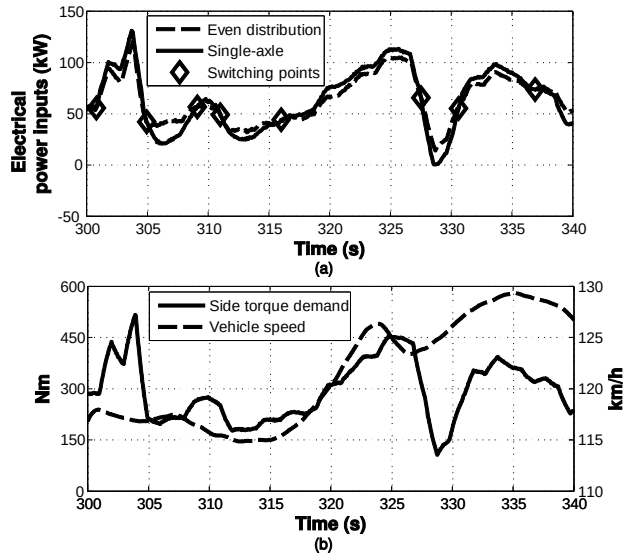

Fig. 7. Sample of driving cycle measurements; (a) electrical power input for the even-distribution and single-axle strategies with the switching points indicated by markers; and (b) side torque demands overlapped with V

The energy consumption of the vehicle with the CA strategy is measured and compared with the ones for the fixed single-axle and even distribution strategies. Table 2 shows the measurement results, which indicate energy savings of up to

~5% for the developed CA algorithm, depending on the driving cycle. Interestingly, the NEDC and Artemis Road favor the single-axle strategy over the even distribution because of the relatively low wheel torque demand. This trend is reversed with the EUDC with 8% slope as it is a more aggressive cycle with mostly high torque demands. The fact that for some conditions the specific vehicle is more efficient with the single-axle strategy is caused by the significant values of the peak power and torque of its electric drivetrains, which work at very low demands during conventional driving cycles.

The operation of the developed torque distribution algorithm over a segment of a driving cycle is investigated in Fig. 7, which confirms the validity of the CA strategy. For instance, between 305 s and 309 s, when the vehicle speed is ~117 km/h, the side torque demand is ~215 Nm, i.e., less than the calculated switching torque of 280 Nm in Fig. 6, and therefore single-axle is the optimal solution, as in Fig. 7(a).

B. Simulations

To examine the performance of the torque distribution strategy in cornering conditions a ramp steer simulation with a validated CarMaker/Simulink vehicle model (see details in [25]) was performed. For the simulation, the vehicle was accelerated to V=110 km/h and, then a constant steering wheel rate of 3 deg/s and up to 100 deg was applied.

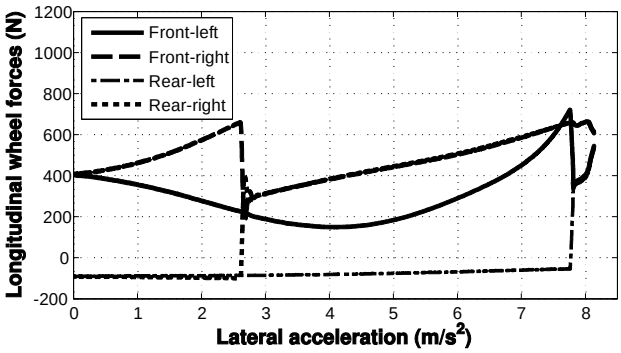

Fig. 8. Longitudinal wheel forces, simulated during the ramp steer maneuver at 100 km/h with the developed CA strategy. The outer and inner sides switch from single-axle to even distributions respectively at a_y of 2.6 and 7.8 m/s^2

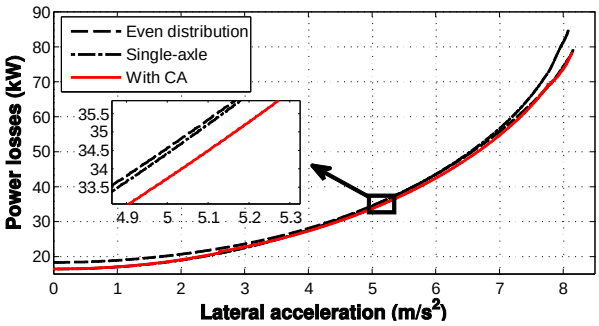

Fig. 9. Total drivetrain power losses (including tire power losses) simulated during the ramp steer maneuver for even torque distribution, single-axle torque distribution, and the developed CA algorithm

Fig. 8 depicts the simulated longitudinal wheel forces as functions of lateral acceleration, a_y, according to the developed CA strategy. The single-axle strategy is the solution for both sides of the vehicle for lateral accelerations below 2.6 m/s^2. For a_y > 7.8 m/s^2, the solution for both sides is the even distribution. Between the two a_y-values the switching between the strategies is dependent on the side of the vehicle – namely, with increasing a_y, the outer side of the vehicle switches earlier to even distribution due to the yaw moment and its contribution to the longitudinal forces in (6). This happens because the specific high-level controller set-up (see Section II.A) applies a yaw moment which reduces vehicle understeer, i.e., the torque demand (the parameter on which the switching is actually based) on the outer side of the car is higher than on the inner side. Therefore, when the lateral acceleration is between 2.6 m/s^2 and 7.8 m/s^2, the torque demand is distributed equally between the front and rear wheels on the outer side and is applied only to the front wheel on the inner side of the vehicle. In other words, 3 motors are simultaneously active.

Fig. 9 shows the total vehicle power loss (excluding the aerodynamic losses) simulated for the three different torque distribution strategies, i.e., even distribution, single-axle, and the developed CA strategy. As with the experimental tests, the CA strategy reduces the drivetrain power losses; here by up to 10% and 8% compared to the even distribution and single-axle strategies. The biggest improvements are achieved at very low and very high lateral accelerations where, respectively, the single-axle strategy and the even distribution strategy are the optimal solutions (see also Fig. 6). For lateral accelerations between 2.6 and 7.8 m/s^2, when the optimal solution for the outer and inner vehicle sides are different (Fig. 8), the developed CA strategy reduces the power loss by ~2.4% (Fig. 9).

V. Conclusion

The presented research work allows the following conclusions, essential for the design of a fast, energy-efficient and easily implementable torque allocation algorithm for four-wheel-drive electric vehicles with equal drivetrains on the front and rear axles:

- For relatively small values of steering wheel angle, the control allocation problem of a four-wheel-drive electric vehicle with multiple motors can be independently solved for the left- and right-hand sides of the vehicle;
- If the power loss characteristics of the electric drivetrains are monotonically increasing functions of the torque demand, the minimum consumption is achieved by using a single motor on each side of the vehicle up to a torque demand threshold, and an even torque distribution among the front and rear motors above such threshold;
- An analytical formula is proposed for the computation of the torque demand threshold, which is a function of vehicle speed, based on the drivetrain power loss characteristic;
- The developed strategy is easily implementable as a small-sized look-up table in the main control unit of the vehicle, allowing real-time operation with minimum demand on the processing hardware;
- The experimental analysis of the case study drivetrain efficiency characteristics as functions of the front-to-total wheel torque distribution confirms the validity of the

proposed control allocation algorithm at different vehicle velocities and torque demands, i.e., at low torques single-axle is the optimal solution and at high torques even distribution is the optimal solution;

- The experimental results for a four-wheel-drive electric vehicle demonstrator along driving cycles show energy consumption reductions between 0.5% and 5%, with respect to the same vehicle with single-axle and even torque distributions;
- The simulation results of ramp steer maneuvers indicate significant energy consumption reductions for the whole range of lateral accelerations.

The approximation related to the assumptions of tire slip ratios similar to those in the rolling road experiments and negligible rolling resistance variation with vertical load will be addressed in future work.

REFERENCES

[1] Y. Wang, B.M. Nguyen, H. Fujimoto, and Y. Hori, "Multirate estimation and control of body sideslip angle for electric vehicles based on onboard vision system," *Industrial Electronics, IEEE Transactions on,* vol. 61, pp. 1133-1143, 2014.

[2] K. Nam, S. Oh, and H. Fujimoto, "Estimation of sideslip and roll angles of electric vehicles using lateral tire force sensors through RLS and Kalman filter approaches, *Industrial Electronics, IEEE Transactions on,* vol. 60, pp. 988-1000, 2013.

[3] Y. Suzuki, Y. Kano, and M. Abe, "A study on tyre force distribution controls for full drive-by-wire electric vehicle," *Vehicle System Dynamics,* vol. 52, pp. 235-250, 2014/05/30 2014.

[4] R. Wang, Y. Chen, D. Feng, X. Huang, and J. Wang, "Development and performance characterization of an electric ground vehicle with independently actuated in-wheel motors," *Journal of Power Sources,* vol. 196, pp. 3962-3971, 2011.

[5] Y. Chen and J. Wang, "Adaptive Energy-Efficient Control Allocation for Planar Motion Control of Over-Actuated Electric Ground Vehicles," *Control Systems Technology, IEEE Transactions on,* vol. 22, pp. 1362-1373, 2014.

[6] A. Pennycott, L. De Novellis, A. Sabbatini, P. Gruber, and A. Sorniotti, "Reducing the motor power losses of a four-wheel drive, fully electric vehicle via wheel torque allocation," *Proceedings of the Institution of Mechanical Engineers, Part D: Journal of Automobile Engineering,* vol. 228, pp. 830-839, 2014.

[7] X. Yuan and J. Wang, "Torque Distribution Strategy for a Front- and Rear-Wheel-Driven Electric Vehicle," *Vehicular Technology, IEEE Transactions on,* vol. 61, pp. 3365-3374, 2012.

[8] L. De Novellis, A. Sorniotti, and P. Gruber, "Wheel Torque Distribution Criteria for Electric Vehicles With Torque-Vectoring Differentials," *Vehicular Technology, IEEE Transactions on,* vol. 63, pp. 1593-1602, 2014.

[9] H. Fujimoto and S. Harada, "Model-Based Range Extension Control System for Electric Vehicles With Front and Rear Driving-Braking Force Distributions," *Industrial Electronics, IEEE Transactions on,* vol. 62, pp. 3245-3254, 2015.

[10] Y. Chen and J. Wang, "Fast and Global Optimal Energy-Efficient Control Allocation With Applications to Over-Actuated Electric Ground Vehicles," *Control Systems Technology, IEEE Transactions on,* vol. 20, pp. 1202-1211, 2012.

[11] Y. Chen and J. Wang, "Design and Experimental Evaluations on Energy Efficient Control Allocation Methods for Overactuated Electric Vehicles: Longitudinal Motion Case," *Mechatronics, IEEE/ASME Transactions on,* vol. 19, pp. 538-548, 2014.

[12] Y. Chen and J. Wang, "Energy-efficient control allocation with applications on planar motion control of electric ground vehicles," in *American Control Conference (ACC), 2011,* San Francisco, CA, 2011, pp. 2719-2724.

[13] S. Fallah, A. Khajepour, B. Fidan, C. Shih-Ken, and B. Litkouhi, "Vehicle Optimal Torque Vectoring Using State-Derivative Feedback and Linear Matrix Inequality," *Vehicular Technology, IEEE Transactions on,* vol. 62, pp. 1540-1552, 2013.

[14] B. Li, A. Goodarzi, A. Khajepour, S.K. Chen, and B. Litkouhi, "An optimal torque distribution control strategy for four-independent wheel drive electric vehicles," *Vehicle System Dynamics,* vol. 53, pp. 1-18, 2015.

[15] P. Tøndel and T. A. Johansen, "Control allocation for yaw stabilization in automotive vehicles using multiparametric nonlinear programming," in *American Control Conference, 2005. Proceedings of the 2005,* 2005, pp. 453-458.

[16] T. A. Johansen, T. P. Fuglseth, P. Tøndel, and T. I. Fossen, "Optimal constrained control allocation in marine surface vessels with rudders," *Control Engineering Practice,* vol. 16, pp. 457-464, 2008.

[17] J. Tjønnås and T. A. Johansen, "Adaptive control allocation," *Automatica,* vol. 44, pp. 2754-2765, 2008.

[18] J. Tjonnas and T. A. Johansen, "Stabilization of Automotive Vehicles Using Active Steering and Adaptive Brake Control Allocation," *Control Systems Technology, IEEE Transactions on,* vol. 18, pp. 545-558, 2010.

[19] T. A. Johansen and T. I. Fossen, "Control allocation—A survey," *Automatica,* vol. 49, pp. 1087-1103, 2013.

[20] O. Härkegård and S. T. Glad, "Resolving actuator redundancy—optimal control vs. control allocation," *Automatica,* vol. 41, pp. 137-144, 2005.

[21] L. F. Domínguez, D. A. Narciso, and E. N. Pistikopoulos, "Recent advances in multiparametric nonlinear programming," *Computers & Chemical Engineering,* vol. 34, pp. 707-716, 2010.

[22] A. Grancharova and T. A. Johansen, "Multi-parametric Programming," in *Explicit Nonlinear Model Predictive Control - Theory and Applications.* vol. 429, ed. Berlin Heidelberg: Springer, 2012, pp. 1-37.

[23] U. Kiencke and L. Nielsen, "Automotive control systems: for engine, driveline, and vehicle," *Measurement Science and Technology,* 2000, 11.12: 1828.

[24] M. Tanelli, S. M. Savaresi, and Carlo Cantoni, "Longitudinal vehicle speed estimation for traction and braking control systems," in *Computer Aided Control System Design, 2006 IEEE International Conference on* Control Applications, pp. 2790-2795.

[25] L. De Novellis, A. Sorniotti, P. Gruber, J. Orus, J.-M. Rodriguez Fortun, J. Theunissen, and J. De Smet, "Direct yaw moment control actuated through electric drivetrains and friction brakes: Theoretical design and experimental assessment," *Mechatronics,* vol. 26, pp. 1-15, 2015.